AD-A121 662 COMPUTATIONAL TREATMENT OF TRANSONIC CANARD-WING INTERACTIONS(U) ROCKWELL INTERNATIONAL THOUSAND OAKS CA V SHANKAR ET AL. JAN 82 AFOSR-TR-82-1007 1/1

UNCLASSIFIED F49620-80-C-0081 F/G 20/4 NL

END

DATE FILMED

DTIC

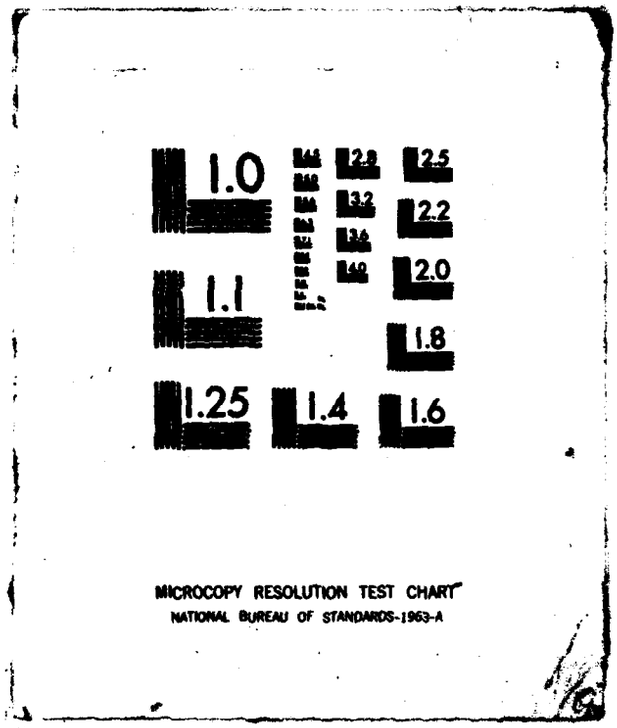
1.0
2.8
2.5
3.2
2.2
3.6
4.0
2.0
1.1
1.8
1.25
1.4
1.6
MICROCOPY RESOLUTION TEST CHART
NATIONAL BUREAU OF STANDARDS-1963-A

UNCLASSIFIED
SECURITY CLASSIFICATION OF THIS PAGE (When Data Entered)

REPORT DOCUMENTATION PAGE

READ INSTRUCTIONS BEFORE COMPLETING FORM

1. REPORT NUMBER: AFOSR-TR- 82-1007	2. GOVT ACCESSION NO.: AD A121662
3. RECIPIENT'S CATALOG NUMBER:	
4. TITLE (and Subtitle): COMPUTATIONAL TREATMENT OF TRANSONIC CANARD-WING INTERACTIONS	5. TYPE OF REPORT & PERIOD COVERED: INTERIM
	6. PERFORMING ORG. REPORT NUMBER:
7. AUTHOR(s): VIJAYA SHANKAR NORMAN MALMUTH	8. CONTRACT OR GRANT NUMBER(s): F49620-80-C-0081
9. PERFORMING ORGANIZATION NAME AND ADDRESS: ROCKWELL INTERNATIONAL SCIENCE CENTER THOUSAND OAKS, CA 91360	10. PROGRAM ELEMENT, PROJECT, TASK AREA & WORK UNIT NUMBERS: 61102F 2307/A1
11. CONTROLLING OFFICE NAME AND ADDRESS: AIR FORCE OFFICE OF SCIENTIFIC RESEARCH/NA BOLLING AFB, DC 20332	12. REPORT DATE: January 1982 13. NUMBER OF PAGES: 8
14. MONITORING AGENCY NAME & ADDRESS(if different from Controlling Office)	15. SECURITY CLASS. (of this report): Unclassified 15a. DECLASSIFICATION/DOWNGRADING SCHEDULE

16. DISTRIBUTION STATEMENT (of this Report)

Approved for Public Release; Distribution Unlimited.

17. DISTRIBUTION STATEMENT (of the abstract entered in Block 20, if different from Report)

DTIC ELECTE NOV 22 1982 S D E

18. SUPPLEMENTARY NOTES

Proceedings of the AIAA Aerospace Sciences Meeting, 20th Orlanda, FL 11-14 Jan 1982, AIAA, 1290 Avenue of the Americas, NY, NY 10104 1982

19. KEY WORDS (Continue on reverse side if necessary and identify by block number)

TRANSONIC FLOW
CANARD-WING
TRANSONIC SMALL DISTURBANCE THEORY

20. ABSTRACT (Continue on reverse side if necessary and identify by block number)

The transonic canard-wing interaction problem is simulated using modified small disturbance (MDS) transonic theory. The wing and the canard are treated in a sheared fine grid system that is embeded in a global Cartesian crude gird. An appropriate far field and asymptotic expression for the velocity potential derived using Green's theorem is implemented. Results are presented for a few canard-wing configurations and compared with available experimental data. The weakening of the wing shock due to the presence of the canard downwash is illustrated in terms of contour plots.

DD FORM 1 JAN 73 1473 EDITION OF 1 NOV 65 IS OBSOLETE

UNCLASSIFIED
SECURITY CLASSIFICATION OF THIS PAGE

An empirical incidence correction for the wing leading edge vortex gives good agreement with experiment at low incidences. For higher angles of attack, the results indicate that a more sophisticated vortex roll-up and induction model is required.

AIAA-82-0161
Computational Treatment of Transonic Canard-Wing Interactions

V. Shankar and N. Malmuth, Rockwell International Science Center, Thousand Oaks, CA

AIAA 20th Aerospace Sciences Meeting

January 11-14, 1982/Orlando, Florida

COMPUTATIONAL TREATMENT OF TRANSONIC CANARD-WING INTERACTIONS

Vijaya Shankar* and Norman Malmuth**
Rockwell International Science Center
Thousand Oaks, California 91360

Abstract

The transonic canard-wing interaction problem is simulated using modified small disturbance (MSD) transonic theory. The wing and the canard are treated in a sheared fine grid system that is embeded in a global Cartesian crude grid. An appropriate far field and asymptotic expression for the velocity potential derived using Green's theorem is implemented. Results are presented for a few canard-wing configurations and compared with available experimental data. The weakening of the wing shock due to the presence of the canard downwash is illustrated in terms of contour plots. An empirical incidence correction for the wing leading edge vortex gives good agreement with experiment at low incidences. For higher angles of attack, the results indicate that a more sophisticated vortex roll-up and induction model is required.

Introduction

A number of highly maneuverable fighter configurations such as the HiMAT, XFV-12A and Forward Swept Wing, have been proposed with closely coupled canard systems which can lead to several advantages such as higher trimmed-lift capability, improved pitching moment characteristics, and reduced trim drag. Also, the geometric characteristics of closely coupled canard configurations offer an improved longitudinal cross-sectional area progression which could result in reduced wave drag at low supersonic speeds. Additional advantages associated with improved side force capability have been reported by Re and Capone[1]. The associated interaction due to such surfaces with the wing as well as those from conventional tail planes involves important nonlinear phenomena in the supercritical speed regime. These effects can significantly change spanwise load distributions as well as the effective incidence field. Corresponding modifications of aerodynamic performance and stability characteristics are therefore to be anticipated not only for fighter configurations, but with tails interacting with large-aspect-ratio wings typical of transport arrangements as well.

To understand clearly the closely coupled canard-wing interference transonic flow fields with emphasis on benefits associated with longitudinal and lateral positioning that have been discussed in the subsonic regime by Lacey[2] and transonic regime by Gloss and Washburn[3], it is essential to develop a computational model that properly simulates the full nonlinear coupling of both surfaces. In this respect, the mutual induction arises naturally in the computational model in contrast to other "immersion" techniques which have been advocated. The latter employs an iterative procedure in which each surface's isolated aerodynamics is alternately corrected for induction from the other. This concept may have some validity for large stagger and gap cases, but may not converge for closely coupled arrangements. In fact, even if convergence is obtained, the result may not be the physically correct solution.

A mutually interacting two-dimenstional canard-wing model based on the Karman-Guderley transonic small disturbance theory is reported in Ref. [4] showing several parametric studies involving canard-wing angles of attack, stagger and gap between the two lifting elements. The objective of the present study is to extend the two-dimensional analysis to three-dimensions by modifying an existing small disturbance theory transonic code for wing-body combinations[5] to include the presence of a canard or tail. The approach is to introduce a separate sheared fine grid box for the canard similar to the one used for the wing. However, the experience from the two-dimensional analysis[4] indicates that erroneous solutions can result from the use of two fine grid box arrangement for very closely coupled canard-wing systems due to placement of the outer boundaries of the fine grid box in strong nonlinear regions of the other surface. To avoid this situation, when the canard is in the close proximity of the wing, a single fine grid box is used that encloses both the lifting surfaces. By contrast, the two fine grid box arrangement is used for mildly coupled canard-wing configurations. Beside the numerical implementation, the paper also includes a detailed analysis of the appropriate far field procedure based on an asymptotic theory. The present paper neglects the downward deflection of the wake, vortex roll-up and leading edge separation phenomena. These can be important effects and are being considered in separate analyses.

Results are shown for a few sample canard-wing configurations and compared with available experimental data.

Equations and Boundary Conditions

The modified form of the transonic classical small disturbance theory in conservation form as used in Ref. [5], will be employed in the current formulation of the canard/tail problem.

$$\left.\begin{aligned}&\left[(1-M_\infty^2\phi_x)-\frac{\gamma+1}{2}M_\infty^{1.75}\phi_x^2+\left(\frac{\gamma-3}{2}\right)M_\infty^2\phi_y^2\right]_x\\&+\left[\phi_y-(\gamma-1)M_\infty^2\phi_x\phi_y\right]_y+\left[\phi_z\right]_z=0\end{aligned}\right\}\qquad(1)$$

The above equation is in the conservation form usually preferred for better shock resolution. Use of Eq. (1) allows one to apply the wing/canard surface boundary conditions at their respective mean chord planes and transfer boundary conditions on the fuselage to a convenient computational prismatic surface. Referring to Figure 1, the boundary conditions on the wing and canard mean plane are given by

*Member Technical Staff, Associate Fellow AIAA.

**Manager, Fluid Dynamics Group, Associate Fellow AIAA.

$$\phi_z(x,y;z_{w,c}^{\pm}) = \frac{1}{M_\infty^{0.25}} \left\{ \frac{dZ_{w,c}(x,y;z_{w,c}^{\pm}}{dx} - \alpha \right\} \quad (2)$$

where $z = z_{w,c}^{\pm}$ defines the wing/canard mean plane with a + sign denoting the upper surface and a - sign the lower surface. The wing/canard shape is prescribed by $Z_{w,c}(x,y)$. Application of boundary conditions on the mean plane avoids the need for body-fitted mapping procedures. The subscripts w and c denote the wing and canard, respectively.

Across the vortex wake, there will be a jump in the velocity potential ϕ which will be incorporated in the calculation as a boundary condition while solving Eq. (1) at grid points neighboring the wake. The wake jump condition is

$$\left.\begin{aligned} [\phi]_{WING} &= \phi(x,y,z_w^+) - \phi(x,y,z_w^-) \\ &= \Gamma_w(y) \quad , \quad x > x_{TE,w} \\ [\phi]_{CANARD} &= \phi(x,y,z_c^+) - \phi(x,y,z_c^-) \\ &= \Gamma_c(y) \quad , \quad x > x_{TE,c} \end{aligned}\right\} \quad (3)$$

where x_{TE} prescribes the trailing edge shape and $\Gamma_w(y)$ and $\Gamma_c(y)$ denote the sectional circulation given by

$$\left.\begin{aligned} \Gamma_w(y) &= \phi(x_{TE,w}(y),y,z_w^+) \\ &\quad - \phi(x_{TE,w}(y),y,z_w^-) \\ \Gamma_c(y) &= \phi(x_{TE,c}(y),y,z_c^+) \\ &\quad - \phi(x_{TE,c}(y),y,z_c^-) \end{aligned}\right\} \quad (4)$$

Transformation and Gridding

In general, canard-wing configurations will have different planform shapes for both lifting units, and in particular, different leading and trailing edge sweeps. In order to treat arbitrary arrangements, it is essential to incorporate separate shearing transformations for both surfaces to unsweep them to rectangular planforms in a computational domain. This can be accomplished using the following shearing transformation.

$$\left.\begin{aligned} \xi_{w,c} &= \frac{x - x_{LE,w,c}(y)}{x_{TE,w,c}(y) - x_{LE,w,c}(y)} \\ \eta_{w,c} &= y \\ \zeta_{w,c} &= z \end{aligned}\right\} \quad (5)$$

Since the transformation for the wing is different from the canard, the computational box containing the canard will be different from that containing the wing. This is illustrated in Figure 2.

In order to establish a communication between the wing box and the canard box for data transfer from one to the other, a global crude grid will be set up which completely encloses both as shown in Figure 2. The global crude grid is in terms of the Cartesian system while the canard and wing grids are in terms of sheared coordinates represented by

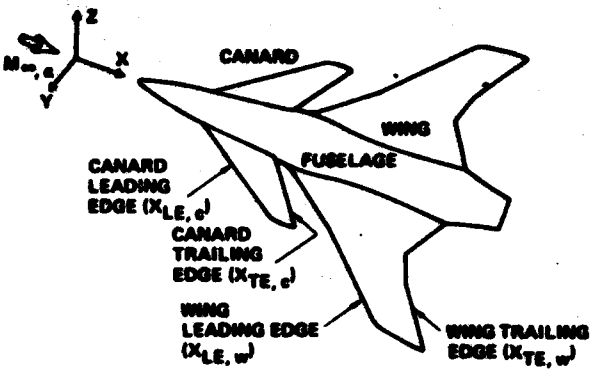

Fig. 1. General canard-wing-fuselage arrangement

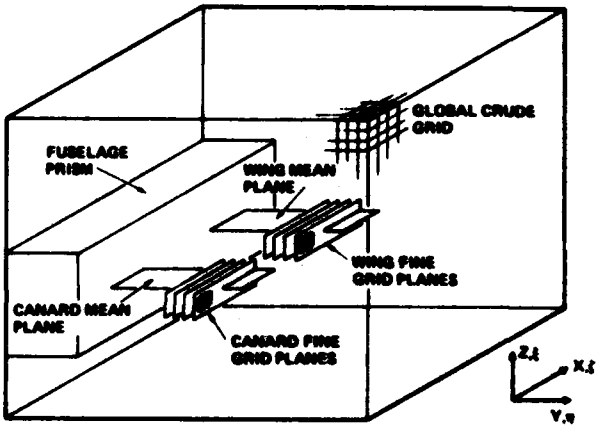

Fig. 2. Computational domain in for the canard-wing-fuselage arrangement

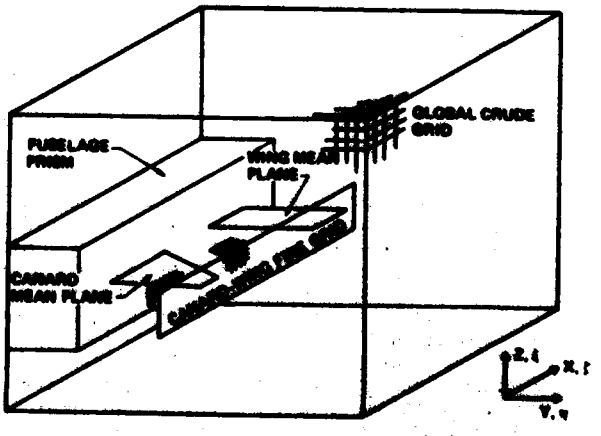

Fig. 3. Single fine grid arrangement

Eq. 5. To achieve a desired flow resolution for the two units, a very fine grid with clustering near the leading and trailing edges will be used in the canard and wing boxes. The Cartesian crude grid will extend several chord lengths away from the configuration where far field boundary conditions can be set. For very closely coupled canard-wing systems the concept of two fine grid box arrangement can lead to erroneous solutions as well as numerical stability problems due to placement of the outer boundaries of the fine grid boxes in strong nonlinear regions of the other surface. This problem was experienced in the earlier two-dimensional analysis[4]. Thus, when a closely coupled canard-wing system is analyzed, a single fine grid box that encloses both the canard and the wing is used (the single fine grid box has a shearing transformation based on the wing planform). This is illustrated in Figure 3. In this situation, the location of the canard leading and trailing edges within the wing sheared fine grid system is obtained by interpolation. Also, the fine grid may have to be specified manually to achieve desired grid clustering for the canard. The double fine grid box arrangement of Figure 2 should work very well for mildly coupled canard-wing systems.

Solution Procedure

Equation (1) in its Cartesian form is solved in the global crude grid while the transformed equation in terms of the new variable ζ,η,ξ is solved in the fine grid box using a successive line over relaxation algorithm. After each relaxation cycle along the crude grid-fine grid interface, the potential values from the crude grid are interpolated on to the fine grid points and used as Dirichlet boundary condition for the fine grid box. Similarly, at the wing and canard mean planes, the potential values for the crude grid points are obtained from the grid values and provide a Dirichlet boundary condition for the crude grid domain. The use of crude grid-fine grid successive sweep procedure accelerates the convergence process[6].

Far Field Solution

Along the outer boundaries of the computational domain it is important to use appropriate far field boundary conditions. These will be obtained from a bi-wing generalization of the asymptotic analysis of Murman and Cole[7] for non-lifting airfoils and its three-dimensional wing extension by Klunker[8].

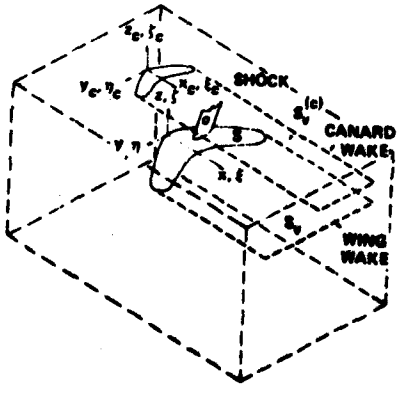

Fig. 4a. Canard-wing system and far-field boundaries

Referring to Figure 4a, a bi-wing system without a fuselage is shown. The far field derivation procedure will be indicated for these elements, and an extension to inclusion of the fuselage will be briefly indicated. Shown in the figure is the canard surface, S_c, upstream of the main wing, S_w. Also depicted are the respective trailing vortex sheets, $S_v^{(c)}$ and S_v, of both elements. A $z=0$ projection of the compound lifting system is indicated in Figure 4b.

For this derivation, we neglect the downward deflection of the wake for moderately large downstream locations of the computational approximation of the Trefftz plane boundary. Also neglected in this treatment are vortex roll-up and leading edge separation phenomena.

Using the procedure from Refs. [7] and [8], we obtain the aforementioned integrodifferential equation for the velocity potential ϕ by applying Green's theorem to the small disturbance equation. Here we deal with the Karman-Guderley formulation to illustrate the basic method to be applied to a modified small disturbance solver[4]. Using suitable strained coordinates (x,y,z) indicated in the figure (for field points referred to an origin at the center of the wing leading edge, and a corresponding set (ξ,η,ζ) for the dummy variables, the small disturbance equation for the perturbation potential ϕ in this system is

$$\left.\begin{aligned} \nabla^2_{\xi,\eta,\zeta}\phi \equiv \frac{\partial^2\phi}{\partial\xi^2} + \frac{\partial^2\phi}{\partial\eta^2} + \frac{\partial^2\phi}{\partial\zeta^2} = A\left(\phi_\xi^2\right)_\xi \\ A \equiv \frac{\gamma+1}{2} \quad . \end{aligned}\right\} \qquad (6)$$

For purposes of application of Green's theorem, we introduce a fundamental solution G which satisfies the following equation

$$\nabla^2_{\xi,\eta,\zeta} G = \delta(\xi-x)\delta(\eta-y)\delta(\zeta-z) \quad . \qquad (7)$$

Thus, G is the usual unit source given by

$$G = -\frac{1}{4\pi R}$$

$$R^2 = (x-\xi)^2 + (y-\eta)^2 + (z-\zeta)^2 \quad .$$

Using Green's theorem on the domain cut along the approximate wake locations shown in Figure 4b, i.e., the planes, $y_c = 0$ and $y = 0$, we obtain

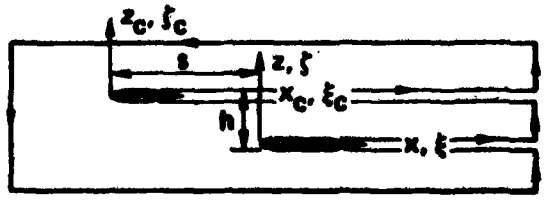

Fig. 4b. Canard-wing system - profile view

$$
\left.
\begin{aligned}
&- \iint_{S_c+S+S_v^{(c)}+S_v} [\phi]G_\zeta \, d\xi d\eta + \iint_{S_c+S} \mathcal{G}[\phi_\zeta] d\xi d\eta \\
&= \phi(x,y,z) + A \int\int\int_{-\infty}^{\infty} \phi_\xi^2 G_\xi \, d\xi d\eta d\zeta
\end{aligned}
\right\} \quad (8)
$$

where, in the partial integrations, all terms from the shock surfaces such as σ (shown schematically in Figure 4a) vanish, and

$$[f(x,y,z)] \equiv f(x,y,0+) - f(x,y,0-)$$

and the ξ,ζ subscripts denote partial differentiation in the integrals.

The integrals over the finite domains can be simplified by approximating the kernels for $x^2 + y^2 + z^2 \to \infty$, with normalized semispan $B = O(y^2 + z^2)$. This approximation and the condition that can be arbitrarily prescribed leads to the desired asymptotic formula

$$\phi = I_L + I_T + I_L^{(c)} + I_T^{(c)} + I_V \qquad (9)$$

where, if the wing and canard are given by the equations,

$$z = f_{u,\ell}(x,y) \quad , \quad (x_{LE} \le x \le x_{TE} \quad , \quad -B \le y \le B)$$

$$z = f_{u,\ell}^{(c)}(x,y) \quad , \quad (x_{LE}^{(c)} \le x \le x_{TE}^{(c)} \quad , \quad -B_c \le y \le B_c)$$

respectively, then

$$I_L = \frac{z\Gamma}{4\pi\rho^2}\left[1 + \frac{x}{R_0}\right] = \text{wing lift contribution} \qquad (10a)$$

$$I_T = \frac{x}{2\pi R_0^3} \iint_S t(\xi,\eta) d\xi d\eta = \text{thickness contribution} \qquad (10b)$$

$$I_V = -A \int\int\int_{-\infty}^{\infty} \phi_\xi^2 G_\xi \, d\xi d\eta d\zeta = \text{nonlinear source} \qquad (10c)$$

$$I_L^{(c)} = \frac{z_c \Gamma_c}{4\pi\rho}\left[1 + \frac{x_c}{R_c}\right] = \text{canard lift} \qquad (10d)$$

$$I_T^{(c)} = \frac{x_c}{2\pi R_{c_0}^3} \iint_{S_c} t_c \, d\xi d\eta = \text{canard thickness} \qquad (10e)$$

with

$$x_c = x - s \quad , \quad z_c = z - h \quad , \quad \rho^2 = x^2 + z^2 \quad ,$$

$$\rho_c^2 = x_c^2 + z_c^2 \quad , \quad t = f_u - f_\ell \quad , \quad t_c = f_u^{(c)} - f_\ell^{(c)} \quad ,$$

$$R^2 = (x-\xi)^2 + (y-\eta)^2 + z^2 \quad , \quad R_0^2 = x^2 + y^2 + z^2 \quad ,$$

$$R_{c_0}^2 = x_c^2 + y^2 + z_c^2 \quad , \quad \Gamma = \int_{-B}^{B} \gamma(\eta) d\eta \quad ,$$

$$\Gamma_c = \int_{-B}^{B_c} \gamma_c(\eta) d\eta \quad , \quad \gamma = [\phi]_{x_{TE}} \quad , \quad \gamma_c = [\phi]_{x_{c_{TE}}} \quad ,$$

and B, B_c representing respectively the scaled wing and canard semispans.

Note that in (9)

$$\left.
\begin{aligned}
I_L &= O(S/R_0) \\
I_L^{(c)} &= O(S_c/R_0)
\end{aligned}
\right\} \quad \text{as } R_0 \to \infty \quad ,$$

and the rest of the terms are higher order being $O(R_0^{-2})$, which can be neglected for sufficiently large computational domains. It is therefore apparent that owing to the linearity of the far field, the dominant effect is the sum of the two lift contributions I_L and I_T. Where, as in the two-dimensional case discussed in Ref. [4], there is however nonlinear coupling between the circulations Γ and Γ_c.

In a similar fashion, the effect of the far field of a slender body contribution can be added to (9) using the nonlinear line source far field expression given in Ref. [9]. Denoting this term as I_F, we have that

$$I_F = O(S_0/R_0) \quad \text{as} \quad R_0 \to \infty$$

where S_0 is the body base area. If, as in typical cases, $S_0/S_c \ll 1$ and $S_c \ll S$, then I_F will be neglected.

In the vicinity of the projections of the lifting elements in the Trefftz plane, the previous approximations become invalid. The appropriate limits are obtained by assuming

$$z, y, z_c = O(B, B_c) \quad \text{as} \quad x \to \infty \quad . \qquad (11)$$

Using the limit (11), (8) can be approximated to give the contribution of the projection of the vortex sheets from both elements

$$
\begin{aligned}
\phi \triangleq \frac{z_c}{2\pi} &\int_{-B_c}^{B_c} \frac{\gamma_c(\eta) d\eta}{(y-\eta)^2 + z_c^2} \\
&+ \frac{z}{2\pi} \int_{-B_w}^{B_w} \frac{\gamma(\eta) d\eta}{(y-\eta)^2 + z^2} \quad , \text{ as } x \to \infty
\end{aligned}
\qquad (12)
$$

Since

$$\lim_{z \to 0} \left\{ \frac{z}{\pi[(y-\eta)^2 + z^2]} \right\} = \delta(y-\eta)\operatorname{sgn} z$$

then

$$\phi(x,y,0\pm) \triangleq \frac{z_c}{2\pi} \int_{-B_c}^{B_c} \frac{\gamma_c(\eta)d\eta}{(y-\eta)^2 + z_c^2} \pm \frac{\gamma(y)}{2}, \quad x \to \infty \quad (13a)$$

and

$$\phi(x,y,h\pm) \pm \frac{\gamma_c(y)}{2} + \frac{z}{2\pi} \int_{-B}^{B} \frac{\gamma(\eta)d\eta}{(y-\eta)^2 + z^2}, \quad x \to \infty \quad (13b)$$

for the fuselage absent.

Equation (12) corresponds to the solution of the cross flow Laplace's equation for the perturbation potential in the Trefftz plane cut about the projections of the wing and canard. If a fuselage is present, the solution can be obtained by superposing the appropriate Trefftz plane limit of the nonlinear line source described in Ref. [9].

Results

All the canard-wing calculations presented here were performed using the LBL CDC 7600 machine. A single fine grid encompassing both the canard and wing was used since the configurations considered in this paper were all very closely coupled canard systems. A typical fine grid consisted of 90x30x20 points and the crude grid 30x20x20 points. A total of 100 crude-fine cycles requiring 10-15 minutes of CPU time usually resulted in satisfactory convergence in which the difference in ϕ between two successive cycles was of the order of 10^{-4}.

Gloss and Washburn[3] have made extensive experimental measurements on the close coupled canard-wing configuration shown in Figure 5. The wing and canard surfaces consisted of sharp leading edge circular arc airfoils. The pressure data in their report clearly indicate a strong leading edge vortex system especially at higher angles of attack. Since the computational model in its present form cannot predict leading edge vortex flows, for comparison purposes, only the small angle of attack case is considered, where the leading edge vortex is weak. Figure 6 shows the comparison of spanload distribution on the wing with and without the presence of the canard. To match the experimental lift, the computer code was run at an angle of attack of 5.8°, while the experiment was conducted at 4.12°. The increased angle of attack used in the computational run, is an ad hoc fix to account for the suction peak associated with the weak leading edge vortex present in the experimental run as well as viscous and wall interference effects. Still, there is a discrepancy in the surface pressure distribution comparison between numerical prediction and experimental data as shown in Figure 7. The presence of the canard produces a downwash field in front of the wing causing an effective decrease in the angle of attack. This results in a reduction in the nose pressure distribution. The comparison on the lower surface pressure with and without the canard is very good. At higher angles of attack the comparison with data is very poor due to the inability of the computational model to predict the leading vortex system. The case shown in Figure 7 at least indicates the right trend predicted by the computational model with the canard present and interestingly, is in qualitative agreement with the behavior of two-dimensional systems treated in Ref. [4].

Another canard-wing configuration considered is shown in Figure 8. Two different canard positions in the vertical direction are analyzed. For this case, the effect of the canard and its position on the wing sectional lift characteristics is shown in Figure 9, for $M_\infty = 0.84$ and angle of attack of 3°. The lift produced by the canard produces a downwash in front of the wing causing the wing lift to decrease. However, at wing span stations away from the canard tip, the effect of the canard is minimal. Corresponding to this case, the pressure contours at the wing span station $(y/b_w) = 0.245$ is shown in Figure 10 for both the canard off and on situations. Figure 10(a) shows the isolated wing case (canard off) exhibiting a shock on the upper surface. When the canard is placed at 0.5 C_R above the wing plane (C_R is the wing root chord), the shock weakening on the wing due to downwash produced by the canard is clear in Figure 10(b). Even further weakening of the shock due to closer positioning of the canard is seen in Figure 10(c). Figure 11 shows the surface pressure distribution on the wing at various span stations with canard off and on. This figure also clearly shows the reduction in wing shock strength when the canard is present.

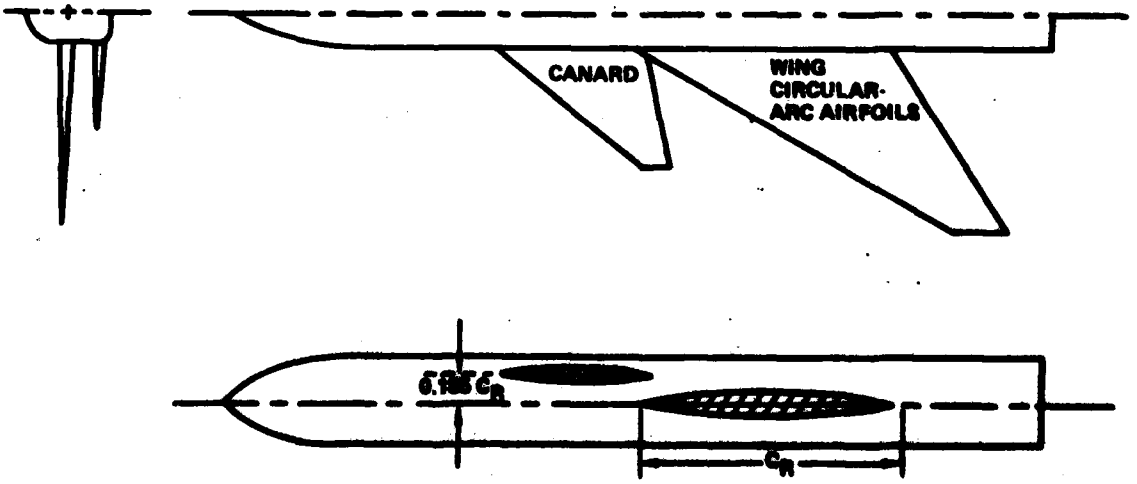

Fig. 5. Closely coupled canard-wing model (Ref. 3)

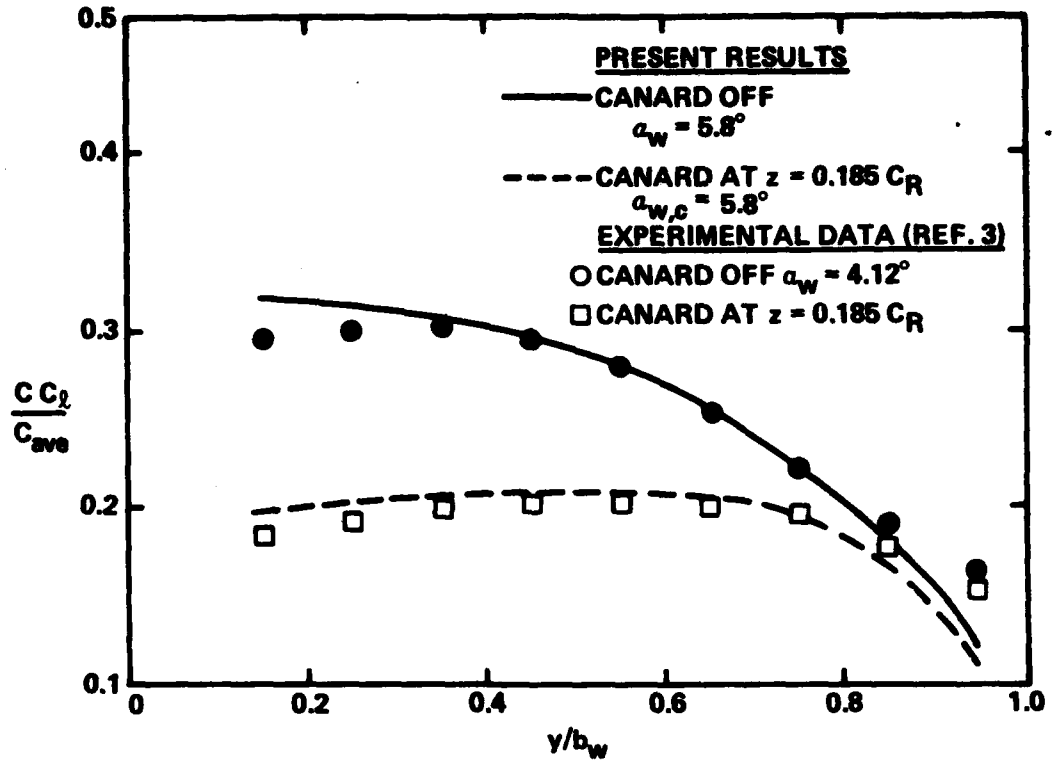

Fig. 6. Effect of canard on spanload distribution
$M_\infty = 0.95$

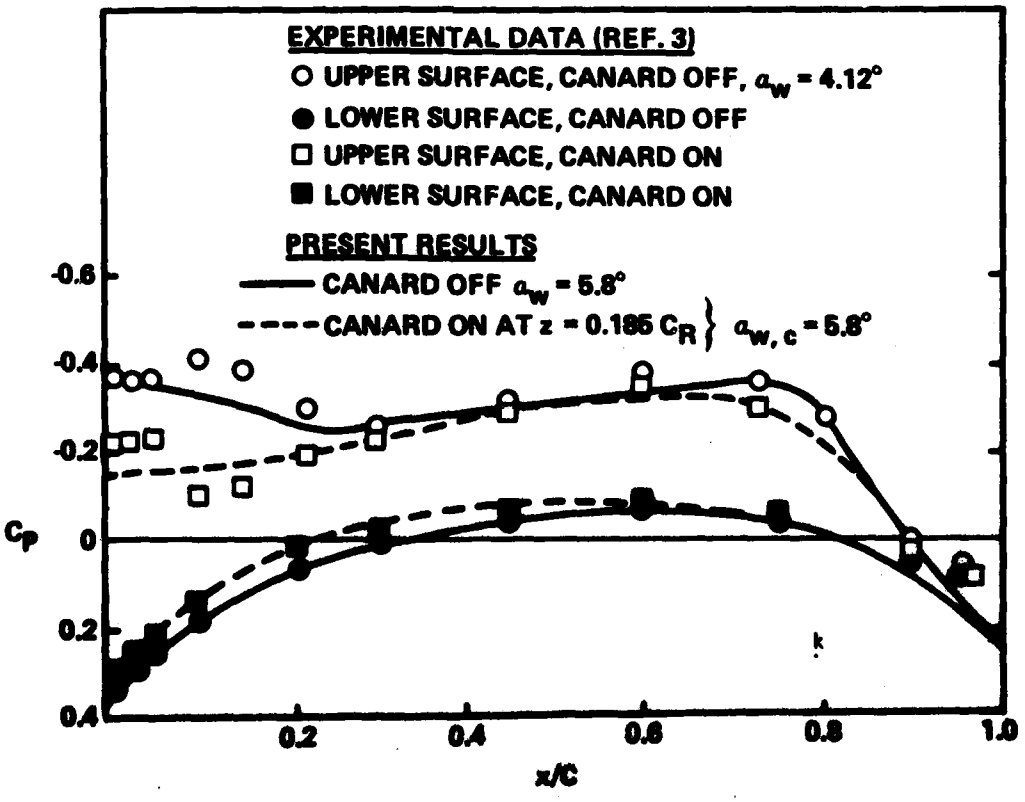

Fig. 7. Effect of canard on wing surface pressures,
$y/b_w = 0.45$, $M_\infty = 0.95$

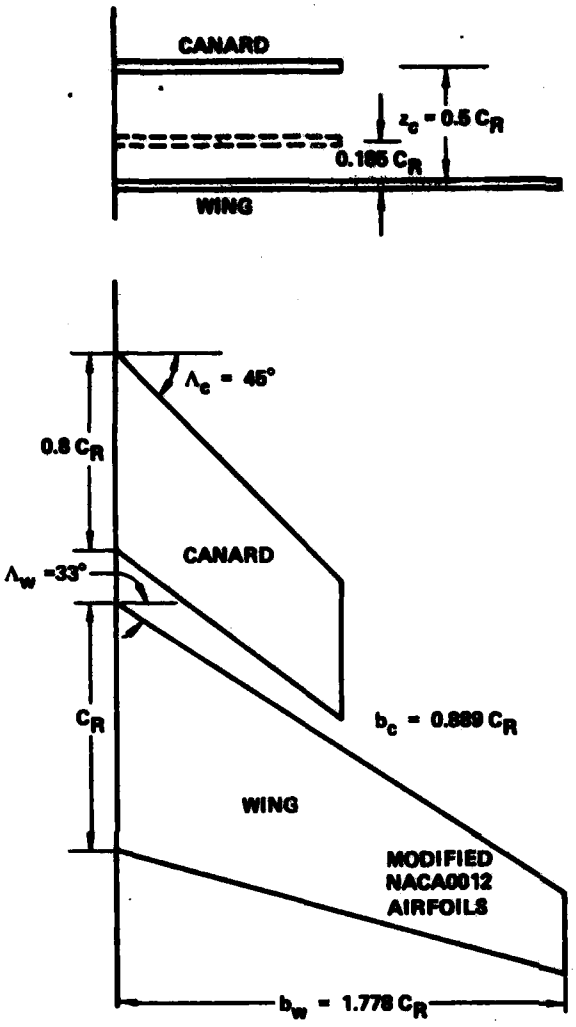

Fig. 8. Canard-wing geometry

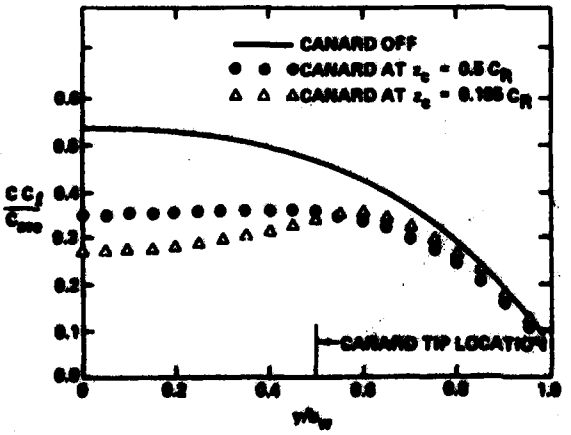

Fig. 9. Wing sectional characteristics with canard off and on. $M_\infty = 0.84$, $\alpha_{c,w} = 3°$

Conclusions

A simple canard-wing transonic computational model is presented. The formulation neglects wake deflection, vortex roll-up and leading edge separation phenomena. An appropriate far field expression for the velocity potential is derived and implemented. Results are presented for two canard-wing configurations and some comparison with experimental data is made. An empirical incidence correction for the wing leading edge vortex gives good agreement with experiment at low incidences. The presence of the canard produces a downwash field that tends to weaken the shock system on the wing surface. For higher incidence, some kind of a leading edge potential vortex core model superimposed onto the present computational treatment would greatly enhance the prediction capability. This will be pursued in the future along with suitable models for incorporating the wake roll-up phenomena. The computational speed can also be enhanced by use of implicit factored algorithms.

Acknowledgement

A portion of the research described in this paper was supported under AFOSR Contract F44620-81-C-0044.

References

1. Re, R.J. and Capone, F.J., "An Investigation of a Close Coupled Canard as a Direct Side Force Generation on a Fighter Model at Mach Numbers from 0.40 to 0.90," NASA Technical Note TN D-8510, July 1977.
2. Lacey, D., "Aerodynamic Characteristics of the Close Coupled Canard as Applied to Low-to-Moderate Swept Wings, Volume 2: Subsonic Speed Regime," David Taylor Model Basin Report DTNSRDC 79/002, January, 1979.
3. Gloss, B.B. and Washburn, K.E., "A Study of Canard-Wing Interference Using Experimental Pressure Data at Transonic Speeds," NASA TP-1355, January, 1979.
4. Shankar, V. and Malmuth, N.D., "Transonic Flow Calculations over Two-Dimensional Canard-Wing Systems," AIAA Paper 79-1565, July, 1979; also to appear in the Journal of Aircraft.
5. Shankar, V., Malmuth, N.D., and Cole, J.D., "Computational Transonic Design Procedure for Three-Dimensional Wings and Wing-Body Combinations," AIAA Paper 79-0344, presented at the AIAA 17th Aerospace Sciences Meeting, New Orleans, Louisiana, January 15-17, 1979.
6. Boppe, C.W. and Stern, M.A., "Simulated Transonic Flows for Aircraft with Nacelles, Pylons and Winglets," AIAA Paper 80-0130, AIAA 18th Aerospace Sciences Meeting, Pasadena, California, January 14-16, 1980.
7. Murman, E.M. and Cole, J.D., "Calculations of Plane Steady Transonic Flows," AIAA Journal, Vol. 9, No. 1, January, 1971.
8. Klunker, E.B., "Contributions to Methods for Calculating the Flow About Thin Lifting Wings at Transonic Speeds - Analytical Expression for the Far Field," NASA TN D-6530, 1971.
9. Krupp, J.A. and Murman, E.M., "Computation of Transonic Flows over Lifting Airfoils and Slender Bodies," AIAA J., 10, 7, July, 1971, pp. 880-886.

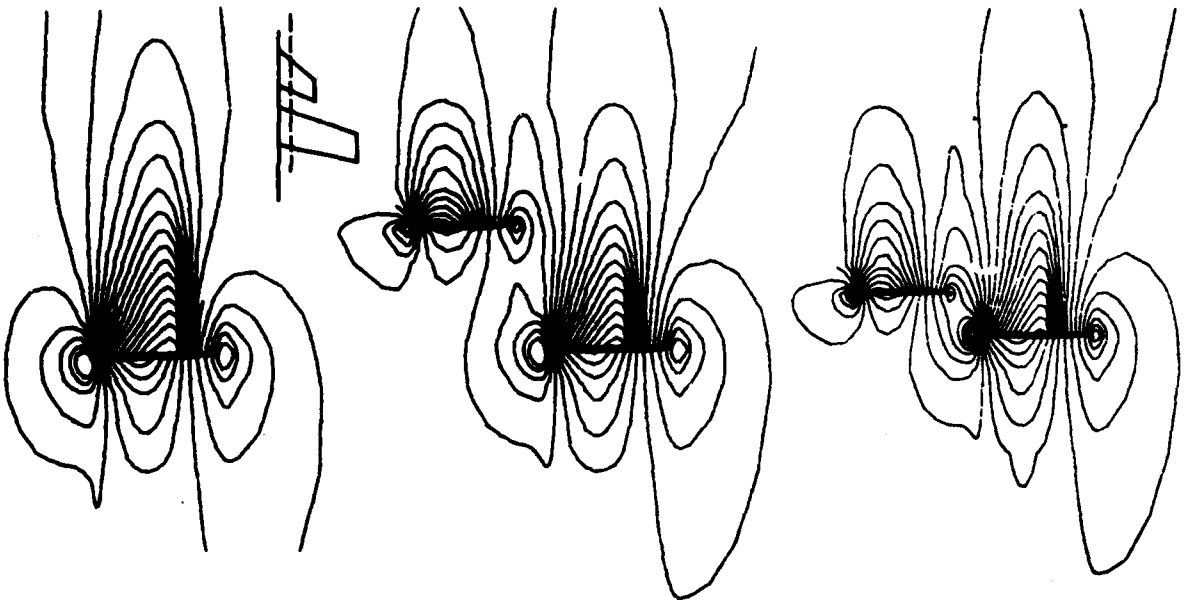

Fig. 10. Constant pressure contours at span station $(y/b_w) = 0.245$. $M_\infty = 0.84$, $\alpha_{w,c} = 3°$

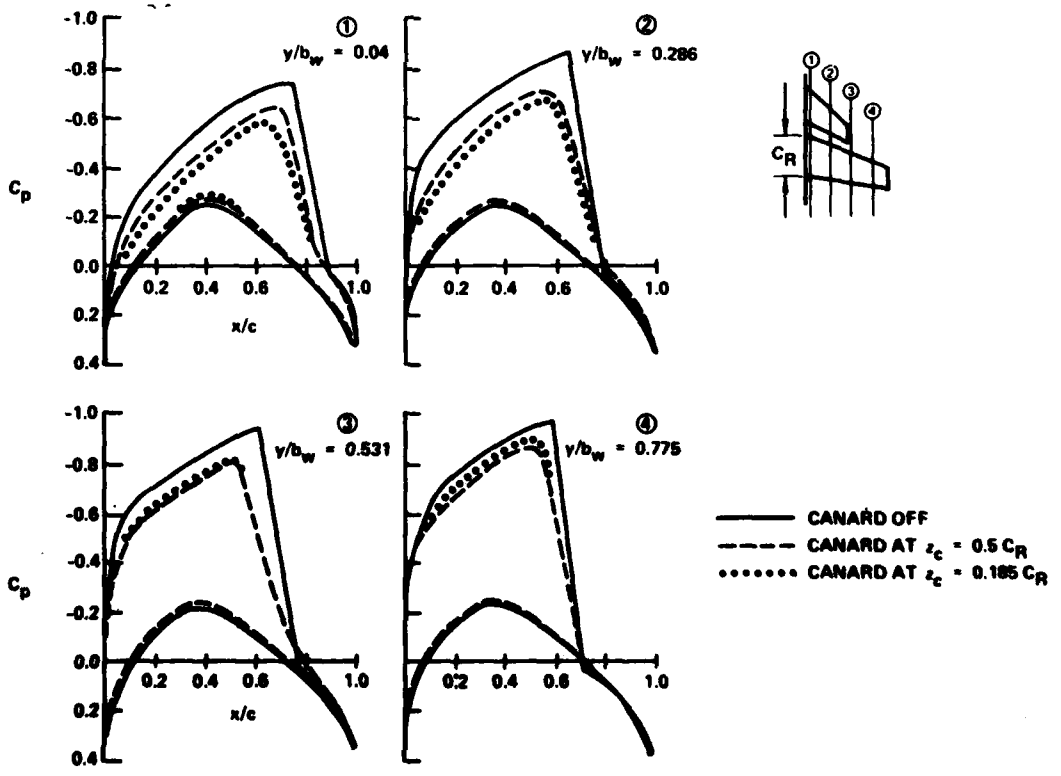

Fig. 11. Surface pressure distribution on the wing with canard off and on. $M_\infty = 0.84$, $\alpha_{c,w} = 3°$